INTERNATIONAL JOURNAL FOR NUMERICAL METHODS IN FLUIDS
Int. J. Numer. Meth. Fluids 2004; **45**:689–714 (DOI: 10.1002/fld.700)

Similarities between the quasi-bubble and the generalized wave continuity equation solutions to the shallow water equations

J. H. Atkinson[1,*,†], J. J. Westerink[1] and J. M. Hervouet[2]

[1]*Department of Civil Engineering and Geological Sciences, University of Notre Dame, Notre Dame, IN 46556, U.S.A.*
[2]*National Hydraulics and Environment Laboratory, Electricité de France, Research and Development Division, 6 Quai Watier, B.P. 49, Chatou 78401, Cedex, France*

SUMMARY

Two common strategies for solving the shallow water equations in the finite element community are the generalized wave continuity equation (GWCE) reformulation and the quasi-bubble velocity approximation. The GWCE approach has been widely analysed in the literature. In this work, the quasi-bubble equations are analysed and comparisons are made between the quasi-bubble approximation of the primitive form of the shallow water equations and a linear finite element approximation of the GWCE reformulation of the shallow water equations. The discrete condensed quasi-bubble continuity equation is shown to be identical to a discrete wave equation for a specific GWCE weighting parameter value. The discrete momentum equations are slightly different due to the bubble function. In addition, the dispersion relationships are shown to be almost identical and numerical experiments confirm that the two schemes compute almost identical results. Analysis of the quasi-bubble formulation suggests a relationship that may guide selection of the optimal GWCE weighting parameter. Copyright © 2004 John Wiley & Sons, Ltd.

KEY WORDS: quasi-bubble; generalized wave continuity equation; shallow water equations; finite elements; dispersion relationship

1. INTRODUCTION

The generalized wave continuity equation (GWCE) formulation and the quasi-bubble approximation are two popular techniques for successfully solving the shallow water equations within a finite element framework. Many early attempts to employ the finite element method for solving the shallow water equations failed because solutions were polluted by large numerical oscillations which obscured the physical solution. For the past 20 years, there has

*Correspondence to: J. H. Atkinson, 3501 Grassland Drive, Norman, OK 73072-2914, U.S.A.
†E-mail: John.H.Atkinson-1@ou.edu

Contract/grant sponsor: U.S. Army Engineer Research and Development Center; contract/grant number: DACW H2-00-C-0006

Published online 19 April 2004

Received 2 October 2002
Revised 20 January 2004

been substantial research in the shallow water community to improve finite element models and this sustained effort is well documented elsewhere [1, 2]. The success of discrete schemes based on the GWCE formulation is due to a monotonic dispersion relationship which yields non-oscillatory solutions [3]. Good results have also been presented for the quasi-bubble scheme [4] but no analysis is available to explain the success of this scheme.

The GWCE method manipulates the primitive shallow water equations in continuum form prior to application of the finite element method, and was first developed by Lynch and Gray [5] and Kinnmark and Gray [6, 7]. The temporal derivative of the continuity equation is combined with the spatially differentiated momentum equations to which a weighted continuity equation is added. The resulting new equation is used instead of the primitive continuity statement. Using the operator notation of Kinnmark [3], the linearized continuity and momentum equations are defined by the following notation:

$$\mathscr{L} \equiv \frac{\partial \zeta}{\partial t} + h\left(\frac{\partial u}{\partial x} + \frac{\partial v}{\partial y}\right) = 0 \tag{1}$$

$$\mathscr{M}_x \equiv \frac{\partial u}{\partial t} + \tau u + g\frac{\partial \zeta}{\partial x} = 0 \tag{2}$$

$$\mathscr{M}_y \equiv \frac{\partial v}{\partial t} + \tau v + g\frac{\partial \zeta}{\partial y} = 0 \tag{3}$$

where u and v are the x and y depth-averaged velocities, ζ the surface elevation, h the bathymetric depth, τ the bottom friction coefficient and g the gravitational acceleration. The GWCE equation is formulated as

$$\begin{aligned}\text{GWCE} &\equiv \frac{\partial \mathscr{L}}{\partial t} - \frac{\partial \mathscr{M}_x}{\partial x} - \frac{\partial \mathscr{M}_y}{\partial y} + G\mathscr{L} = 0 \\ &= \frac{\partial^2 \zeta}{\partial t^2} + G\frac{\partial \zeta}{\partial t} - gh\left(\frac{\partial^2 \zeta}{\partial x^2} + \frac{\partial^2 \zeta}{\partial y^2}\right) + (G - \tau)h\left(\frac{\partial u}{\partial x} + \frac{\partial v}{\partial y}\right) = 0\end{aligned} \tag{4}$$

The new equation possesses second derivatives in time and space which gives the appearance of the classical 'wave equation', and is what gives the technique its name. The constant G is a numerical parameter that controls the balance of wave equation and primitive continuity equation. As $G \to 0$, the equation becomes a pure wave equation, and when $G \gg 0$, the equation reduces to the primitive continuity equation.

Extensive analysis of the GWCE has demonstrated that the scheme is stable and leads to a monotonic dispersion relationship [3, 6–10]. The GWCE approach has been successful because the monotonic dispersion relationship means that the solution does not inherently generate a second artificial high wave number solution associated with spurious modes. The GWCE formulation has been very successful for a wide range of applications.

The quasi-bubble concept adds resolution to the velocity approximation while preserving the standard linear elevation discretization and was first introduced by Mewis and Holz [11]. New velocity nodes are added to the centre of existing finite elements and interpolation for velocity is re-defined. A traditional bubble function enhances the velocity discretization

with the addition of a quadratic interpolating function which has the appearance of a bubble which provides the concept's name. However, the quasi-bubble discretization employs a linear approximation of the bubble, hence 'quasi' bubble [11]. The FE velocity space is enriched by the additional velocity node at the centroid of each triangle and by subdividing each triangle into three linear velocity subtriangles.

The quasi-bubble scheme has been widely exercised as part of the Telemac model which has been developed, and is used extensively, by Electricité de France (EDF) [12–14]. The Telemac algorithm is based upon a standard Galerkin approach. Results have been presented that appear well behaved and undamped, but no rigorous analysis has been presented [4]. Moreover, no dispersion characteristics have been presented in the literature.

In this paper, truncation error analysis and Fourier-based dispersion analysis are employed in one and two dimensions to examine and compare the behaviour of the two schemes. For this study, attention is restricted to solutions of the harmonic form of the governing equations. The harmonic continuity equation is

$$(\hat{\mathrm{i}}\omega)\zeta + h\left(\frac{\partial u}{\partial x} + \frac{\partial v}{\partial y}\right) = 0 \tag{5}$$

and the x and y momentum equations are

$$(\hat{\mathrm{i}}\omega + \tau)us + g\frac{\partial \zeta}{\partial x} = 0 \tag{6}$$

and

$$(\hat{\mathrm{i}}\omega + \tau)v + g\frac{\partial \zeta}{\partial y} = 0 \tag{7}$$

where ω is the temporal frequency and $\hat{\mathrm{i}} \equiv \sqrt{-1}$. The harmonic GWCE is

$$(\hat{\mathrm{i}}\omega)(\hat{\mathrm{i}}\omega + G)\zeta + (G - \tau)h\left(\frac{\partial u}{\partial x} + \frac{\partial v}{\partial y}\right) - gh\left(\frac{\partial^2 \zeta}{\partial x^2} + \frac{\partial^2 \zeta}{\partial y^2}\right) = 0 \tag{8}$$

and is used in conjunction with the two-dimensional harmonic form of the momentum equations. Spatial discretizations are applied to the harmonic form of the governing equations. By casting the equations into harmonic form, the effects of a finite element spatial discretization may be evaluated independently from the choice of time-stepping algorithm. Note that the solutions for the harmonic equations should be the same as the solutions from a consistent time-stepping algorithm with $\Delta t \to 0$.

The formal order of convergence of the discrete approximations for each scheme may be found by substituting a Taylor series expansion for the nodal unknowns. When this is done, some of the terms cancel and what remains is called the modified equation and is the actual equation which the discrete equations approximate. A discrete scheme is consistent if the modified equation reduces to the original differential equation as the grid spacing tends to zero. The terms that appear in the modified equation in addition to the terms from the original differential equation define the truncation error terms.

The dispersion relationship is found through a well-established method [8, 9, 15–17] of performing a Fourier expansion for the nodal unknowns that appear in the discrete equations. Since the governing equations are linear, the solution may be examined by analysing the

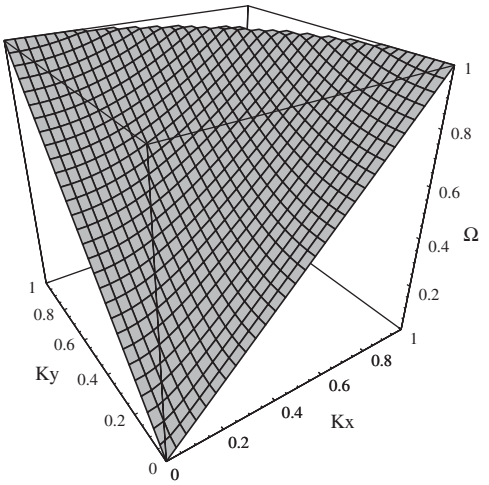

Figure 1. Two-dimensional dispersion surface for the continuum equations.

behaviour of one Fourier component. The dispersion relationship for the continuous linearized shallow water equations is

$$\omega = \frac{\hat{\imath}\tau}{2} \pm \sqrt{gh(k_x^2 + k_y^2) - \left(\frac{\tau}{2}\right)^2} \tag{9}$$

where k_x and k_y are the two wave numbers [1]. Allowing $\tau \to 0$ and defining the non-dimensional variables

$$\Omega \equiv \frac{\omega L}{\pi\sqrt{gh}} \tag{10}$$

$$K_x \equiv \frac{k_x \Delta x}{\pi} \tag{11}$$

and

$$K_y \equiv \frac{k_y \Delta y}{\pi} \tag{12}$$

permits the magnitude of the analytical dispersion relationship to be expressed as

$$\Omega = \left(\frac{L}{\Delta x}\right)\left(K_x^2 + \left(\frac{\Delta x}{\Delta y}\right)^2 K_y^2\right)^{1/2} \tag{13}$$

and is shown in Figure 1 for $L = \Delta x = \Delta y$. The continuum relationship is monotonic everywhere. The dispersion surfaces for the discrete schemes will all be compared with this surface.

2. ONE-DIMENSIONAL EQUATIONS

2.1. Quasi-bubble scheme

Discretization of the one-dimensional form of Equations (5) and (6) with the quasi-bubble enrichment for the velocity space is achieved in one-dimension by adding a velocity node in the centre of each element and associating linear basis and weight functions for the velocity on the refined velocity grid. Elevation unknowns are defined only at the inter-element nodes, but the velocity unknowns are defined at the inter-element nodes and the centre nodes. Thus, the velocity approximation is defined on a grid with twice the resolution of the elevation grid. The weighting and interpolating functions are all equal to the standard linear chapeau functions with the caveat that the functions used for velocity have non-zero support over half the distance of the elevation functions.

The weighted residual statement for the governing equations weights the continuity equation with ϕ_j

$$\int_\Omega \left((\hat{\mathrm{i}}\omega)\zeta + h\frac{\partial u}{\partial x} \right) \phi_j \, \mathrm{d}\Omega = 0 \tag{14}$$

and the momentum equation with ψ_m

$$\int_\Omega \left((\hat{\mathrm{i}}\omega + \tau)u + g\frac{\partial \zeta}{\partial x} \right) \psi_m \, \mathrm{d}\Omega = 0 \tag{15}$$

where $j = 1, \ldots, \mathrm{NPE}$ and $m = 1, \ldots, \mathrm{NPU}$. The two sets of basis functions, $\phi(x)$ and $\psi(x)$, are functions of the spatial co-ordinate x and are used to expand elevation and velocity

$$\zeta(x) \simeq \sum_{j=1}^{\mathrm{NPE}} \zeta_j \phi_j \tag{16}$$

and

$$u(x) \simeq \sum_{m=1}^{\mathrm{NPU}} u_m \psi_m \tag{17}$$

where NPE is the number of elevation nodes and NPU is the number of velocity unknowns.

When the approximations of Equations (16) and (17) are used, the discrete system may be written using implied summation on repeated indices

$$\begin{aligned} \mathbf{ME}_{jk}\zeta_k + \mathbf{B}_{jn}u_n &= 0 \\ \mathbf{MU}_{mn}u_n + \mathbf{C}_{mk}\zeta_k &= 0 \end{aligned} \tag{18}$$

With the four matrices,

$$\mathbf{ME}_{jk} \equiv (\hat{\mathrm{i}}\omega) \int_{\Omega_e} \phi_j \phi_k \, \mathrm{d}x \tag{19}$$

$$\mathbf{MU}_{mn} \equiv (\hat{\mathrm{i}}\omega + \tau) \int_{\Omega_e} \psi_m \psi_n \, \mathrm{d}x \tag{20}$$

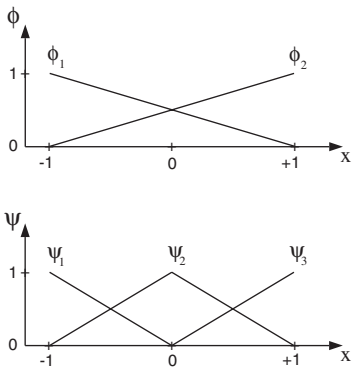

Figure 2. The one-dimensional basis functions for elevation and velocity.

$$\mathbf{B}_{jn} \equiv h \int_{\Omega_e} \phi_j \frac{\partial \psi_n}{\partial x} \, \mathrm{d}x \tag{21}$$

$$\mathbf{C}_{mk} \equiv g \int_{\Omega_e} \psi_m \frac{\partial \phi_k}{\partial x} \, \mathrm{d}x \tag{22}$$

To populate the matrices and complete the discrete scheme, the basis functions must be defined and the integrals evaluated. To simplify the integrations, the basis functions are defined on a master element in a local co-ordinate system, s, such that

$$s \in [-1, 1] \tag{23}$$

for each element. The basis functions for the master element are illustrated in Figure 2 and have the following definitions. The elevation bases are

$$\begin{aligned} \phi_1 &= \tfrac{1}{2}(1 - s) \\ \phi_2 &= \tfrac{1}{2}(1 + s) \end{aligned} \tag{24}$$

and the velocity bases are defined piecewise

$$\begin{aligned} \psi_1 &= \begin{cases} -s & \text{for } s \in -1 < s < 0 \\ 0 & \text{for } s \in 0 < s < 1 \end{cases} \\ \psi_2 &= \begin{cases} 1 + s & \text{for } s \in -1 < s < 0 \\ 1 - s & \text{for } s \in 0 < s < 1 \end{cases} \\ \psi_3 &= \begin{cases} 0 & \text{for } s \in -1 < s < 0 \\ s & \text{for } s \in 0 < s < 1 \end{cases} \end{aligned} \tag{25}$$

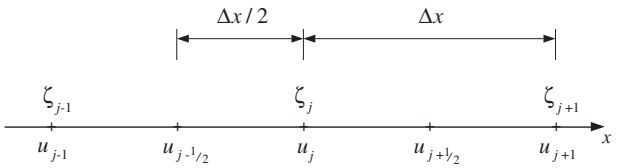

Figure 3. Portion of a one-dimensional grid.

Using the above definitions, the elemental matrices are

$$\mathbf{ME}_{jk} = (\hat{\mathrm{i}}\omega)\frac{\Delta x}{6}\begin{bmatrix} 2 & 1 \\ 1 & 2 \end{bmatrix} \tag{26}$$

$$\mathbf{MU}_{mn} = (\hat{\mathrm{i}}\omega + \tau)\frac{\Delta x}{12}\begin{bmatrix} 2 & 1 & 0 \\ 1 & 4 & 1 \\ 0 & 1 & 2 \end{bmatrix} \tag{27}$$

$$\mathbf{B}_{jn} = \frac{h}{4}\begin{bmatrix} -3 & 2 & 1 \\ -1 & -2 & 3 \end{bmatrix} \tag{28}$$

$$\mathbf{C}_{mk} = \frac{g}{4}\begin{bmatrix} -1 & 1 \\ -2 & 2 \\ -1 & 1 \end{bmatrix} \tag{29}$$

A global system of unknowns is generated by summing the contributions from all the elements, accounting for inter-element C_0 functional continuity and incorporating elevation and velocity boundary conditions at the appropriate nodes. The discrete equations at an interior node for a one-dimensional partition of the x-axis into non-overlapping elements, as in Figure 3, may be summarized by the following three equations. The elevation equation for node j is

$$(\hat{\mathrm{i}}\omega)\frac{\Delta x}{6}(\zeta_{j-1} + 4\zeta_j + \zeta_{j+1}) + \frac{h}{4}(u_{j+1} - u_{j-1}) + \frac{h}{2}(u_{j+1/2} - u_{j-1/2}) = 0 \tag{30}$$

The momentum equation for node j is

$$(\hat{\mathrm{i}}\omega + \tau)\frac{\Delta x}{12}(u_{j-1/2} + 4u_j + u_{j+1/2}) + \frac{g}{4}(\zeta_{j+1} - \zeta_{j-1}) = 0 \tag{31}$$

and the momentum equation for node $j + 1/2$ is

$$(\hat{\mathrm{i}}\omega + \tau)\frac{\Delta x}{12}(u_j + 4u_{j+1/2} + u_{j+1}) + \frac{g}{2}(\zeta_{j+1} - \zeta_j) = 0 \tag{32}$$

Owing to the local support of the elemental quasi-bubble function which is identically zero outside of its element, the momentum equations associated with the centre node only involve nodal unknowns from one element. This permits a static condensation procedure [18] in which the bubble function unknowns may be eliminated at the element level. The procedure is to substitute the momentum equations for the $j\pm\frac{1}{2}$ velocity nodes into the discrete jth momentum and continuity equations. In this way the $j\pm\frac{1}{2}$ variables do not appear, and the global discrete continuity stencil for the ζ_j unknowns becomes

$$(\hat{\mathrm{i}}\omega)\frac{\Delta x}{6}(\zeta_{j-1}+4\zeta_j+\zeta_{j+1})-\frac{3}{4}\frac{gh}{\Delta x(\hat{\mathrm{i}}\omega+\tau)}(\zeta_{j-1}-2\zeta_j+\zeta_{j+1})$$
$$+\frac{h}{8}(u_{j+1}-u_{j-1})=0 \tag{33}$$

while the new discrete stencil for u_j is

$$(\hat{\mathrm{i}}\omega+\tau)\frac{\Delta x}{12}(-u_{j-1}+14u_j-u_{j+1})+\frac{g}{2}(\zeta_{j+1}-\zeta_{j-1})=0 \tag{34}$$

After substituting the Taylor series expanded around node j into Equation (33), the modified quasi-bubble momentum equation is

$$(\hat{\mathrm{i}}\omega)\zeta+\frac{h}{4}\frac{\partial u}{\partial x}-\frac{3}{4}\frac{gh}{(\hat{\mathrm{i}}\omega+\tau)}\frac{\partial^2\zeta}{\partial x^2}$$
$$+(\Delta x)^2\left(\frac{(\hat{\mathrm{i}}\omega)}{6}\frac{\partial^2\zeta}{\partial x^2}-\frac{gh}{16(\hat{\mathrm{i}}\omega+\tau)}\frac{\partial^4\zeta}{\partial x^4}+\frac{h}{24}\frac{\partial^3 u}{\partial x^3}\right)+\text{H.O.T.}=0 \tag{35}$$

for which the spatial truncation error is $O((\Delta x)^2)$. Substituting the Taylor series into Equation (34) results in the modified momentum equation

$$(\hat{\mathrm{i}}\omega+\tau)u+g\frac{\partial\zeta}{\partial x}+\Delta x^2\left(\frac{(\mathrm{i}\omega+\tau)}{12}\frac{\partial^2 u}{\partial x^2}+\frac{g}{6}\frac{\partial^3\zeta}{\partial x^3}\right)+\text{H.O.T.}=0 \tag{36}$$

which also has a second-order leading truncation error term.

2.2. GWCE scheme

The discrete GWCE has been derived elsewhere [3, 5], and the derivation will not be repeated here. The one-dimensional, harmonic version of the GWCE is

$$(\mathrm{i}\omega)(\mathrm{i}\omega+G)\zeta+(G-\tau)h\frac{\partial u}{\partial x}-gh\frac{\partial^2\zeta}{\partial x^2}=0 \tag{37}$$

Equal-order, linear basis and weighting functions are used to discretize Equation (37) and the one-dimensional form of Equation (6). The discrete equations for each node j are the

discrete GWCE

$$(\hat{\imath}\omega)(\hat{\imath}\omega + G)\frac{1}{6}(\zeta_{j-1} + 4\zeta_j + \zeta_{j+1}) - \frac{gh}{\Delta x^2}(\zeta_{j-1} - 2\zeta_j + \zeta_{j+1})$$
$$+(G - \tau)\frac{h}{2\Delta x}(u_{j+1} - u_{j-1}) = 0 \tag{38}$$

and the discrete momentum equation

$$\frac{(\hat{\imath}\omega + \tau)}{6}(u_{j-1} + 4u_j + u_{j+1}) + \frac{g}{2\Delta x}(\zeta_{j+1} - \zeta_{j-1}) = 0 \tag{39}$$

The modified equations for both of these discrete equations are $O((\Delta x)^2)$.

The leading order and subsequent truncation terms for the quasi-bubble condensed modified continuity Equation (35) can be shown to be identical to the corresponding truncation errors in the modified GWCE equation. This can be readily ascertained by directly comparing the two discrete stencils.

2.3. Similarity of the discrete stencils

The discrete GWCE shown in Equation (38) is very similar to the discrete quasi-bubble stencil in Equation (33). If Equation (38) is rewritten by multiplying both sides by Δx and dividing by $\hat{\imath}\omega + G$ to yield

$$(\hat{\imath}\omega)\frac{\Delta x}{6}(\zeta_{j-1} + 4\zeta_j + \zeta_{j+1}) - \frac{gh}{\Delta x(\hat{\imath}\omega + G)}(\zeta_{j-1} - 2\zeta_j + \zeta_{j+1})$$
$$+\frac{(G - \tau)}{(\hat{\imath}\omega + G)}\frac{h}{2}(u_{j+1} - u_{j-1}) = 0 \tag{40}$$

then a term-by-term comparison may be made with Equation (33). Equating the coefficients of the second and third terms in Equations (40) and (33) yields two relationships for G. Both relationships lead to the constraint

$$G = \frac{\hat{\imath}\omega + 4\tau}{3} \tag{41}$$

Substituting this value for G into the discrete GWCE results in exactly the same equation as the discrete quasi-bubble equation (33). Consequently, the quasi-bubble discretization for elevation is shown to be equivalent to a discrete GWCE with a specific value of G.

It is also noted that the discrete stencils for the momentum equation for the GWCE implementation, Equation (39), and for the quassi-bubble implementation, Equation (34), are identical with the exception of the mass matrix terms. For a lumped formulation, both equations would be identical.

2.4. Dispersion analysis

The dispersion properties are an indication of propagation characteristics and more importantly reveal whether a scheme excites a dual wave number response. Since the governing equations are linear, the solution may be examined by analysing the behaviour of one generic Fourier mode. This permits the dependent variable at a node j to be replaced by the Fourier mode

$$\begin{aligned} u_j &= u^o \mathrm{e}^{\hat{\mathrm{i}}kx_j} = u^o \mathrm{e}^{\hat{\mathrm{i}}k(j\Delta x)} \\ \zeta_j &= \zeta^o \mathrm{e}^{\hat{\mathrm{i}}kx_j} = \zeta^o \mathrm{e}^{\hat{\mathrm{i}}k(j\Delta x)} \end{aligned} \tag{42}$$

where k is the wave number. The x_j co-ordinate is expressed in terms of the distance from a reference node, and the result when the Fourier substitution is made is a square matrix system for the Fourier amplitudes, ζ^o and u^o. For a non-trivial solution to exist, the determinant of the matrix must equal zero, and this constraint yields a relation between the wave number k and the harmonic frequency ω.

When the Fourier substitutions are made into the pair of discrete quasi-bubble equations given by Equations (34) and (33), the matrix system obtained for the ζ^o and u^o Fourier amplitudes is

$$\begin{bmatrix} \hat{\mathrm{i}}\omega(\hat{\mathrm{i}}\omega - \tau)\beta_2 + \frac{9}{2}\frac{gh}{\Delta x^2}\beta_1 & \hat{\mathrm{i}}\,\frac{3h}{4\Delta x}(\hat{\mathrm{i}}\omega - \tau)\alpha \\ \hat{\mathrm{i}}\,\dfrac{6g}{\Delta x}\alpha & (\hat{\mathrm{i}}\omega + \tau)\beta_3 \end{bmatrix} \begin{Bmatrix} \zeta^o \\ u^o \end{Bmatrix} = \begin{Bmatrix} 0 \\ 0 \end{Bmatrix} \tag{43}$$

Constraining the determinant produces the dispersion relationship

$$\omega = \left(\frac{\hat{\mathrm{i}}\tau}{2}\right) \pm \left(\frac{9}{2}\frac{gh}{\Delta x^2}\left[\frac{\beta_1}{\beta_2} + \frac{\alpha^2}{\beta_2\beta_3}\right] - \left(\frac{\tau}{2}\right)^2\right)^{1/2} \tag{44}$$

where

$$\beta_1 = \cos(k\Delta x) - 1 \tag{45}$$

$$\beta_2 = \cos(k\Delta x) + 2 \tag{46}$$

$$\beta_3 = 7 - \cos(k\Delta x) \tag{47}$$

$$\alpha = \sin(k\Delta x) \tag{48}$$

The non-dimensional variables in Equations (10) and (11) may be used to cast Equation (44) into non-dimensional form. With $\tau \to 0$ the magnitude of the non-dimensional dispersion relationship for the quasi-bubble scheme is

$$\Omega = \left(\frac{9}{2\pi^2}\left[\frac{\beta_1}{\beta_2} + \frac{\alpha^2}{\beta_2\beta_3}\right]\right)^{1/2} \tag{49}$$

When the Fourier substitutions are made into the discrete GWCE scheme, the following system is obtained for the Fourier amplitudes for a generic value of G:

$$\begin{bmatrix} -\frac{\omega}{6}(\omega - \hat{\mathrm{i}}G)\beta_2 - \frac{gh}{\Delta x^2}\beta_1 & \hat{\mathrm{i}}\,\frac{h}{2\Delta x}(G-\tau)\alpha \\ \hat{\mathrm{i}}\,\frac{g}{2\Delta x}\alpha & (\hat{\mathrm{i}}\omega + \tau)\frac{\beta_2}{6} \end{bmatrix} \begin{Bmatrix} \zeta^o \\ u^o \end{Bmatrix} = \begin{Bmatrix} 0 \\ 0 \end{Bmatrix} \tag{50}$$

where β_1, β_2, and α are given in Equations (45), (46) and (48). When $G = \tau$ is substituted into Equation (50), the dispersion relationship is

$$\omega = \left(\frac{\mathrm{i}\tau}{2}\right) \pm \left(\frac{6gh}{\Delta x^2}\left[\frac{-\beta_1}{\beta_2}\right] - \left(\frac{\tau}{2}\right)^2\right)^{1/2} \tag{51}$$

When $\tau \to 0$, non-dimensionalizing yields

$$\Omega = \left(\frac{6}{\pi^2}\left[\frac{-\beta_1}{\beta_2}\right]\right)^{1/2} \tag{52}$$

The GWCE dispersion relationship depends upon the value of G [19]. In the previous section, it was demonstrated that the discrete quasi-bubble equations are nearly identical to a GWCE formulation for a specific selection of G. Consequently, it is desired to compare the dispersion relationships of these two schemes when Equation (41) is satisfied. Substituting Equation (41) into (50) and setting the determinant to zero yields the dispersion relationship

$$\omega_{qbG} = \left(\frac{\hat{\mathrm{i}}\tau}{2}\right) \pm \left(27\,\frac{gh}{\Delta x^2}\left[\frac{\beta_2}{6\beta_1} + \frac{12\alpha^2}{\beta_1^2}\right] - \left(\frac{\tau}{2}\right)^2\right)^{1/2} \tag{53}$$

which may be expressed in non-dimensional variables. When $\tau \to 0$ the magnitude of the non-dimensional dispersion relationship is

$$\Omega_{qbG} = \left(\frac{27}{\pi^2}\left[\frac{\beta_2}{6\beta_1} + \frac{12\alpha^2}{\beta_1^2}\right]\right)^{1/2} \tag{54}$$

The non-dimensional dispersion relationships for the continuum solution, the quasi-bubble scheme and the GWCE scheme with $G = \tau$, $G = (\hat{\mathrm{i}}\omega + 4\tau)/3$, and $G = \infty$ are plotted in Figure 4. One sees that the dispersion curves for the quasi-bubble and GWCE schemes are very similar. As expected, the dispersion relationship for the GWCE scheme with the appropriate G value does compare very closely with the quasi-bubble dispersion curve. The quasi-bubble curve is still slightly closer to the analytical curve over most of the wave number range, but the two relationships are very close and are identical as $K \to 0$ and 1. As the value of G increases, it is well known that the GWCE dispersion curve will begin bending down toward the primitive relation and in the limit as $G \to \infty$, the GWCE dispersion curve will fold completely to zero and recover the dispersion curve associated with a linear finite element discretization of the primitive equations. Kolar *et al.* [19] showed that optimal values for G are in the range $G = \tau \to 10\tau$ and for G is much larger than 10τ that oscillatory solutions result due to degradation of the dispersion properties. Moreover, it has been empirically observed that satisfying mass conservation requires a lower limit of acceptable G values of $G \sim 0.0001$

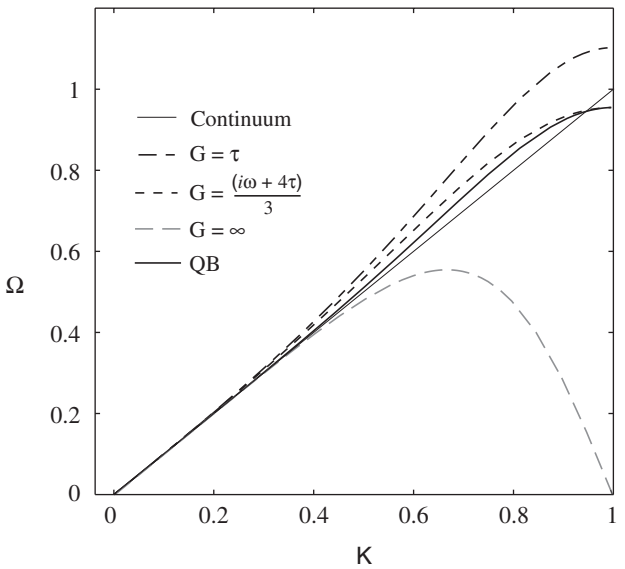

Figure 4. Dispersion relationships for the quasi-bubble (QB), GWCE with $G=\tau$, GWCE with $G=(\hat{\imath}\omega+4\tau)/3$, $G=\infty$ and continuum equations.

in deep water. The value of G suggested by Equation (41) gives very similar values to what has been empirically found. Figure 4 shows that the GWCE scheme has optimal dispersion properties for G very close to the value given by the expression in Equation (41). For values much lower than this G, the dispersion curve is too high. For values much higher than this G, the dispersion relationship begins to fold and the monotonic properties diminish. The dispersion curve for the quasi-bubble scheme closely approximates the analytical curve over a large range of wave numbers, and where deviations occur, they are small. Thus, it appears that the quasi-bubble discretization 'chooses' the value of G which yields optimal dispersion properties.

3. TWO-DIMENSIONAL EQUATIONS

3.1. Quasi-bubble equations

The derivation of the discrete quasi-bubble scheme in two dimensions is very similar to the one-dimensional derivation. The continuity equation is weighted with the elevation basis and the momentum equations are weighted with the velocity basis, yielding one constraint for each elevation node and one constraint for each velocity node. The discrete scheme may be written as

$$\begin{aligned} \mathbf{ME}_{jk}\zeta_k + \mathbf{Ax}_{jn}u_n + \mathbf{Ay}_{jn}v_n &= 0 \\ \mathbf{MU}_{mn}u_n + \mathbf{Bx}_{mk}\zeta_k &= 0 \\ \mathbf{MU}_{mn}v_n + \mathbf{By}_{mk}\zeta_k &= 0 \end{aligned} \tag{55}$$

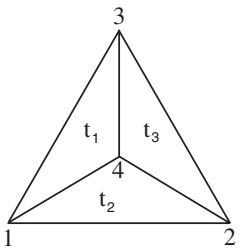

Figure 5. The triangular quasi-bubble master element.

The matrices will be populated by assembling the contributions from each element and by performing the integrations on a triangular master element. The elevation basis is defined on the standard triangular finite element and the functions are the standard linear finite element basis functions. The velocity basis functions are re-defined on a new master element, shown in Figure 5. The new triangle has an additional node located at the centroid of the element and three sub-triangles within it. There is an x and y velocity value for each node and a set of standard linear basis function associated with each sub-triangle. Thus, the quasi-bubble basis function is piecewise linear. Developing the element matrices associated with the velocity basis proceeds by assembling contributions from the three sub-triangles exactly as one assembles standard elements. It is not necessary to define explicitly the co-ordinates of the quasi-bubble nodes when creating a finite element grid of the domain. A standard finite element grid is all that is necessary. When the integrations are required, an element of the grid is mapped to the standard master element, which is further divided as in Figure 5. The elemental velocity 'mass' matrix is

$$\begin{aligned}\mathbf{MU}_{ij} &= (\hat{\mathrm{i}}\omega + \tau)\int_{\Omega} \psi_i\psi_j \,\mathrm{d}\Omega \\ &= (\hat{\mathrm{i}}\omega + \tau)\left(\int_{t_1} \psi_i\psi_j \,\mathrm{d}\Omega + \int_{t_2} \psi_i\psi_j \,\mathrm{d}\Omega + \int_{t_3} \psi_i\psi_j \,\mathrm{d}\Omega\right) \\ &= (\hat{\mathrm{i}}\omega + \tau)\frac{A_e}{36}\begin{bmatrix} 4 & 1 & 1 & 2 \\ 1 & 4 & 1 & 2 \\ 1 & 1 & 4 & 2 \\ 2 & 2 & 2 & 6 \end{bmatrix}\end{aligned} \tag{56}$$

where A_e is the area of element e. The same piecewise strategy is used to populate the other matrices in Equation (55). The following definitions are used for the x and y nodal differences

$$\begin{aligned} a_1 &= x_3 - x_2 \quad a_4 = x_4 - x_2 \quad a_7 = x_4 - x_3 \\ a_2 &= x_1 - x_3 \quad a_5 = x_3 - x_4 \quad a_8 = x_4 - x_1 \\ a_3 &= x_2 - x_1 \quad a_6 = x_1 - x_4 \quad a_9 = x_2 - x_4 \end{aligned} \tag{57}$$

and

$$\begin{aligned} b_1 &= y_2 - y_3 \quad b_4 = y_2 - y_4 \quad b_7 = y_3 - y_4 \\ b_2 &= y_3 - y_1 \quad b_5 = y_4 - y_3 \quad b_8 = y_1 - y_4 \\ b_3 &= y_1 - y_2 \quad b_6 = y_4 - y_1 \quad b_9 = y_4 - y_2 \end{aligned} \tag{58}$$

Using the above variables, the elemental matrices are

$$\begin{aligned} \mathbf{Ax}_{jm} &\equiv h \int_{\Omega_e} \phi_j \frac{\partial \psi_m}{\partial x} \, \mathrm{d}\Omega \\ &= \frac{h}{18} \begin{bmatrix} 4b_1 & 4b_6 + b_7 & 4b_8 + b_9 & -3b_1 \\ 4b_4 + b_5 & 4b_2 & b_8 + 4b_9 & -3b_2 \\ b_4 + 4b_5 & b_6 + 4b_7 & 4b_3 & -3b_3 \end{bmatrix} \end{aligned} \tag{59}$$

$$\begin{aligned} \mathbf{Ay}_{jm} &\equiv h \int_{\Omega_e} \phi_j \frac{\partial \psi_m}{\partial y} \, \mathrm{d}\Omega \\ &= \frac{h}{18} \begin{bmatrix} 4a_1 & 4a_6 + a_7 & 4a_8 + a_9 & -3a_1 \\ 4a_4 + a_5 & 4a_2 & a_8 + 4a_9 & -3a_2 \\ a_4 + 4a_5 & a_6 + 4a_7 & 4a_3 & -3a_3 \end{bmatrix} \end{aligned} \tag{60}$$

$$\begin{aligned} \mathbf{Bx}_{mj} &\equiv g \int_{\Omega_e} \psi_m \frac{\partial \phi_j}{\partial x} \, \mathrm{d}\Omega \\ &= \frac{g}{18} \begin{bmatrix} 2b_1 & 2b_2 & 2b_3 \\ 2b_1 & 2b_2 & 2b_3 \\ 2b_1 & 2b_2 & 2b_3 \\ 3b_1 & 3b_2 & 3b_3 \end{bmatrix} \end{aligned} \tag{61}$$

$$\begin{aligned} \mathbf{By}_{mj} &\equiv g \int_{\Omega_e} \psi_m \frac{\partial \phi_j}{\partial y} \, \mathrm{d}\Omega \\ &= \frac{g}{18} \begin{bmatrix} 2a_1 & 2a_2 & 2a_3 \\ 2a_1 & 2a_2 & 2a_3 \\ 2a_1 & 2a_2 & 2a_3 \\ 3a_1 & 3a_2 & 3a_3 \end{bmatrix} \end{aligned} \tag{62}$$

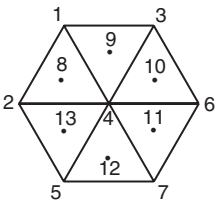

Figure 6. A patch of six equilateral triangle elements.

and

$$\mathbf{ME}_{ij} \equiv \hat{\mathrm{i}}\omega \int_{\Omega_e} \phi_i \phi_j \, \mathrm{d}\Omega$$

$$= (\hat{\mathrm{i}}\omega) \frac{A_e}{12} \begin{bmatrix} 2 & 1 & 1 \\ 1 & 2 & 1 \\ 1 & 1 & 2 \end{bmatrix} \tag{63}$$

To assemble a representative discrete equation in two dimensions, a configuration of elements must be considered. The elemental contributions from each of the six triangles shown in Figure 6 will be assembled into a discrete equation for the centre node in the patch of elements. The discrete continuity equation for node 4 is

$$\begin{aligned} &\hat{\mathrm{i}}\omega(\zeta_1 + \zeta_2 + \zeta_3 + 6\zeta_4 + \zeta_5 + \zeta_6 + \zeta_7) \\ &\quad + \frac{h}{\Delta x}\left(\frac{2}{3}(u_3 - u_1) + \frac{2}{3}(u_7 - u_5) + \frac{4}{3}(u_6 - u_2) + (u_{11} - u_9) + (u_{12} - u_8)\right) \\ &\quad + \frac{h}{\Delta y}(2(v_1 - v_5) + 2(v_3 - v_7) + (v_8 - v_9) + (v_{12} - v_{11}) + (v_{13} - v_{10})) = 0 \end{aligned} \tag{64}$$

The discrete x and y momentum equations for node 4 are

$$\begin{aligned} &(\hat{\mathrm{i}}\omega + \tau)(u_1 + u_2 + u_3 + 12u_4 + u_5 + u_6 + u_7 + u_8 + u_9 + u_{10} + u_{12} + u_{13}) \\ &\quad + 2\frac{g}{\Delta x}((\zeta_3 - \zeta_1) + (\zeta_7 - \zeta_5) + 2(\zeta_6 - \zeta_2)) = 0 \end{aligned} \tag{65}$$

and

$$\begin{aligned} &(\hat{\mathrm{i}}\omega + \tau)(v_1 + v_2 + v_3 + 12v_4 + v_5 + v_6 + v_7 + v_8 + v_9 + v_{10} + v_{12} + v_{13}) \\ &\quad + 2\frac{g}{\Delta y}((\zeta_1 - \zeta_5) + (\zeta_3 - \zeta_7)) = 0 \end{aligned} \tag{66}$$

The quasi-bubble node numbers are 8–13, each having an x and y momentum equation pair associated with it. The u and v velocities associated with them all have the same form. The equations for node 8 will be presented as typical:

$$u_8 = \frac{g}{\Delta x(\hat{\imath}\omega + \tau)}(\zeta_2 - \zeta_4) - \frac{1}{3}(u_1 + u_2 + u_4) \tag{67}$$

$$v_8 = 2\frac{g}{\Delta y(\hat{\imath}\omega + \tau)}((\zeta_2 - \zeta_1) + (\zeta_4 - \zeta_1)) - \frac{1}{3}(v_1 + v_2 + v_4) \tag{68}$$

The expressions for the quasi-bubble nodes only contain values from the three vertices of the triangle in which they are located. Consequently, they may be eliminated from Equations (64)–(66) as in the one-dimensional derivation. The resulting system includes the elevation and velocity values at nodes 1–7 only. The quasi-bubble nodal values could be recovered as a post-processing step once the calculation is complete. When the quasi-bubble values are eliminated, the three discrete equations for node 4 at the centre of the patch of elements are, for ζ,

$$\begin{aligned}
&(\hat{\imath}\omega)(\zeta_1 + \zeta_2 + \zeta_3 + 6\zeta_4 + \zeta_5 + \zeta_6 + \zeta_7) \\
&\quad + \frac{2gh}{(\hat{\imath}\omega + \tau)\Delta y^2}(-2(\zeta_1 + \zeta_3) + (\zeta_2 + 6\zeta_4 + \zeta_6) - 2(\zeta_5 - \zeta_7)) \\
&\quad + \frac{8gh}{(\hat{\imath}\omega + \tau)\Delta x^2}(-\zeta_2 + 2\zeta_4 - \zeta_6) + \frac{2h}{3\Delta x}((u_3 - u_1) + 2(u_6 - u_2) + (u_7 - u_5)) \\
&\quad + \frac{h}{\Delta y}((v_3 - v_7) + (v_1 - v_5)) = 0
\end{aligned} \tag{69}$$

and for u and v

$$\begin{aligned}
&(\hat{\imath}\omega + \tau)(u_1 + u_2 + u_3 + 30u_4 + u_5 + u_6 + u_7) \\
&\quad + 6\frac{g}{\Delta x}((\zeta_3 - \zeta_1) + 2(\zeta_6 - \zeta_2) + (\zeta_7 - \zeta_5)) = 0
\end{aligned} \tag{70}$$

and

$$\begin{aligned}
&(\hat{\imath}\omega + \tau)(v_1 + v_2 + v_3 + 30v_4 + v_5 + v_6 + v_7) \\
&\quad + 9\frac{g}{\Delta y}((\zeta_1 - \zeta_5) + (\zeta_3 - \zeta_7)) = 0
\end{aligned} \tag{71}$$

Now one can examine the leading order truncation error associated with the discrete quasi-bubble equations. The modified equation for elevation, found after substituting the Taylor-

series expansions for ζ, u, and v about node 4 into Equation (69), is

$$(\hat{\imath}\omega)\zeta + \frac{1}{3}h\left(\frac{\partial u}{\partial x} + \frac{\partial v}{\partial y}\right) - \frac{2}{3}\frac{gh}{(\hat{\imath}\omega + \tau)}\left(\frac{\partial^2 \zeta}{\partial x^2} + \frac{\partial^2 \zeta}{\partial y^2}\right) + O((\Delta x)^2, \Delta x \Delta y, (\Delta y)^2) = 0 \quad (72)$$

As was the case for the one-dimensional equations, the quasi-bubble modified elevation equation is very similar to the modified GWCE. In fact truncation errors can be shown to be identical for a specific selection of G. Furthermore, the modified momentum equations can be shown to be $O((\Delta x)^2, (\Delta y)^2)$.

3.2. Similarity to the discrete GWCE

It was shown previously that the one-dimensional discrete quasi-bubble continuity equation was equivalent to a one-dimensional discrete GWCE for a specific value of G. To demonstrate that equivalency exists between the two schemes in two dimensions, consider the discrete GWCE for node 4,

$$\begin{aligned}
&(\hat{\imath}\omega)(\zeta_1 + \zeta_2 + \zeta_3 + 6\zeta_4 + \zeta_5 + \zeta_6 + \zeta_7) \\
&\quad + 3\frac{gh}{(\hat{\imath}\omega + G)\Delta y^2}(-2(\zeta_1 + \zeta_3) + (\zeta_2 + 6\zeta_4 + \zeta_6) - 2(\zeta_5 + \zeta_7)) \\
&\quad + 12\frac{gh}{(\hat{\imath}\omega + G)\Delta x^2}(-\zeta_2 + 2\zeta_4 - \zeta_6) \\
&\quad + \frac{(G - \tau)}{(\hat{\imath}\omega + G)}\frac{2h}{\Delta x}((u_3 - u_1) + 2(u_6 - u_2) + (u_7 - u_5)) \\
&\quad + \frac{(G - \tau)}{(\hat{\imath}\omega + G)}\frac{3h}{\Delta y}((v_1 - v_5) + (v_3 - v_7)) = 0
\end{aligned} \quad (73)$$

Observe that the nodal unknowns appear in identical combinations in Equations (69) and (73) with differences only in the preceding coefficients. Equating the coefficients yields four relationships:

$$\frac{(G - \tau)}{(\mathrm{i}\hat{\omega} + G)}\frac{2h}{\Delta x} = \frac{2h}{3\Delta x} \quad (74)$$

$$\frac{(G - \tau)}{(\mathrm{i}\hat{\omega} + G)}\frac{3h}{\Delta y} = \frac{h}{\Delta y} \quad (75)$$

$$\frac{12}{(\hat{\imath}\omega + G)}\frac{gh}{\Delta x^2} = \frac{8}{(\hat{\imath}\omega + \tau)}\frac{gh}{\Delta x^2} \quad (76)$$

and

$$\frac{3}{(\hat{\imath}\omega + G)}\frac{gh}{\Delta x^2} = \frac{2}{(\hat{\imath}\omega + \tau)}\frac{gh}{\Delta x^2}$$

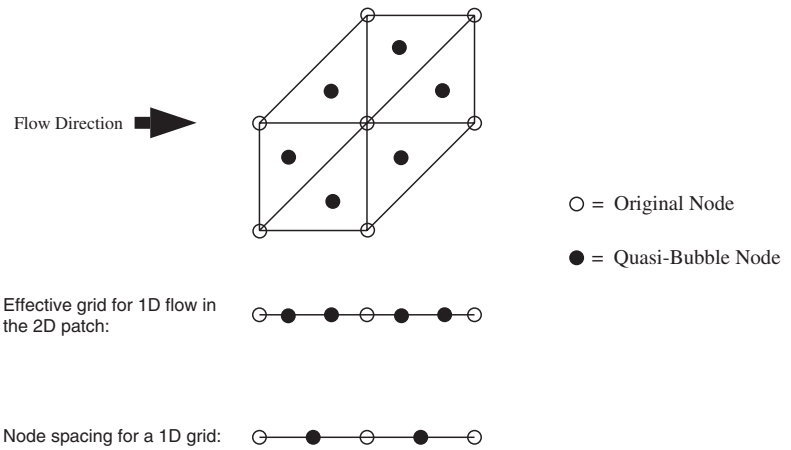

Figure 7. The difference between effective two-dimensional node spacing and one-dimensional node spacing for quasi-bubble grids.

Solving for G in any of these four constraints leads to the same relationship for G given by

$$G = \frac{(\hat{\imath}\omega + 3\tau)}{2} \tag{77}$$

When this value of G is used, the discrete GWCE stencil of Equation (73) becomes identical to the discrete quasi-bubble continuity stencil of Equation (59). Consequently, the one-dimensional finding extends to two dimensions and the quasi-bubble approximation may be seen to be equivalent to a GWCE formulation with a specific value of G. This also means Equations (73) and (69) have identical truncation error.

The expression in Equation (77) is a slightly different relationship than Equation (41) obtained from the discrete one-dimensional equations. The origin of this subtle difference is found in the two-dimensional quasi-bubble formulation where the distribution of nodes is always different from a one-dimensional quasi-bubble formulation. Consider the effect of an assumed one-dimensional flow in the x-direction through the grid patch shown in Figure 7, and note the grid spacing seen by the discrete stencil. A one-dimensional grid is also shown, for which the additional quasi-bubble nodes are in the centre of the element, resulting in an effective grid doubling. The additional nodes for the two-dimensional triangles result in an effective grid refinement that is more than a doubling. For this reason, the two-dimensional discrete continuity equation will never reduce exactly to the one-dimensional stencil. This effective grid refinement explains the difference in one and two dimensional relationships for G. Despite the difference in the two expressions, they are still very similar. With actual values for ω and τ, very similar values of G are computed from each expression. For example, with $\omega = 0.0001$ and $\tau = 0.0003$ Equation (41) gives $G = 0.000401$ and Equation (77) gives $G = 0.000453$. Each relationship expresses a similar physical balance.

3.3. Dispersion analysis

Following the strategy outlined in Reference [1], the dispersion relationship for the discrete quasi-bubble scheme and GWCE scheme can be developed. After the Fourier modes

$$\begin{aligned}\zeta_j &= \zeta^o \mathrm{e}^{\hat{\mathrm{i}}k_x x_j + \hat{\mathrm{i}}k_y y_j} = \zeta^o \mathrm{e}^{\hat{\mathrm{i}}k_x(j\Delta x) + \hat{\mathrm{i}}k_y(j\Delta y)} \\ u_j &= u^o \mathrm{e}^{\hat{\mathrm{i}}k_x x_j + \hat{\mathrm{i}}k_y y_j} = u^o \mathrm{e}^{\hat{\mathrm{i}}k_x(j\Delta x) + \hat{\mathrm{i}}k_y(j\Delta y)} \\ v_j &= v^o \mathrm{e}^{\hat{\mathrm{i}}k_x x_j + \hat{\mathrm{i}}k_y y_j} = v^o \mathrm{e}^{\hat{\mathrm{i}}k_x(j\Delta x) + \hat{\mathrm{i}}k_y(j\Delta y)}\end{aligned} \tag{78}$$

are substituted into the set of discrete quasi-bubble equations given by Equations (69)–(71) the system matrix for the Fourier amplitudes is

$$\begin{bmatrix} (\hat{\mathrm{i}}\omega)(\beta_2+3) - \dfrac{8gh}{(\hat{\mathrm{i}}\omega+\tau)\Delta x^2}\beta_2 - \dfrac{2gh}{(\hat{\mathrm{i}}\omega+\tau)\Delta y^2}\beta_3 & \hat{\mathrm{i}}\dfrac{2h}{3\Delta x}\alpha_1 & \hat{\mathrm{i}}\dfrac{h}{\Delta y}\alpha_2 \\ \hat{\mathrm{i}}\dfrac{6g}{\Delta x}\alpha_1 & (\hat{\mathrm{i}}\omega+\tau)(\beta_1+15) & 0 \\ \hat{\mathrm{i}}\dfrac{9g}{\Delta y}\alpha_2 & 0 & (\hat{\mathrm{i}}\omega+\tau)(\beta_1+15) \end{bmatrix} \tag{79}$$

When the determinant of the system matrix is set to zero, the dispersion relationship for the discrete quasi-bubble scheme is obtained:

$$\begin{aligned}\omega_{\mathrm{qb}} = \left(\frac{\hat{\mathrm{i}}\tau}{2}\right) \pm \Bigg[&\left(4\frac{gh}{\Delta x^2}\right)\left(\frac{2\beta_2}{\beta_1+3} - \frac{\alpha_1^2}{(\beta_1+3)(\beta_1+15)}\right) \\ &+ \left(\frac{gh}{\Delta y^2}\right)\left(\frac{2\beta_3}{\beta_1+3} - \frac{9\alpha_2^2}{(\beta_1+3)(\beta_1+15)}\right) - \left(\frac{\tau}{2}\right)^2 \Bigg]^{1/2}\end{aligned} \tag{80}$$

The trigonometric constants are

$$\begin{aligned}\beta_1 &= \cos(k_x\Delta x) + \cos\left(\frac{k_x\Delta x}{2} + k_y\Delta y\right) + \cos\left(\frac{k_x\Delta x}{2} - k_y\Delta y\right) \\ \beta_2 &= \cos(k_x\Delta x) + 1 \\ \beta_3 &= 2\cos\left(\frac{k_x\Delta x}{2} + k_y\Delta y\right) + 2\cos\left(\frac{k_x\Delta x}{2} - k_y\Delta y\right) - \cos(k_x\Delta x) - 3 \\ \alpha_1 &= \sin\left(\frac{k_x\Delta x}{2} + k_y\Delta y\right) + \sin\left(\frac{k_x\Delta x}{2} - k_y\Delta y\right) + 2\sin(k_x\Delta x) \\ \alpha_2 &= \sin\left(\frac{k_x\Delta x}{2} + k_y\Delta y\right) - \sin\left(\frac{k_x\Delta x}{2} - k_y\Delta y\right)\end{aligned} \tag{81}$$

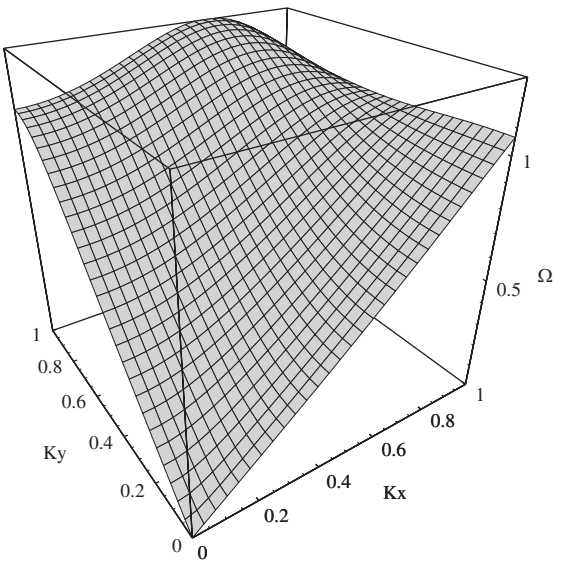

Figure 8. Two-dimensional dispersion surface for the quasi-bubble scheme.

When $\tau \to 0$ and using the non-dimensional variables presented in Equations (10)–(12), the non-dimensional quasi-bubble dispersion relationship is

$$\Omega_{\mathrm{qb}} = \frac{1}{\pi}\sqrt{\frac{4\alpha_1^2 + 3\alpha_2^2}{(\beta_1 + 3)(\beta_1 + 15)} - \frac{16(\beta_1 - 3)}{3(\beta_1 + 3)}} \tag{82}$$

which is shown in Figure 8.

The GWCE dispersion relationship was derived in Reference [8]. With the same trigonometric constants as in Equation (81), the GWCE dispersion relationship is

$$\omega_{\mathrm{GWCE}} = \left(\frac{\hat{\mathrm{i}}\tau}{2}\right) \pm \left(\frac{gh}{\beta_1}\left[\frac{12}{\Delta x^2}\beta_2 + \frac{3}{\Delta y^2}\beta_3\right] - \left(\frac{\tau}{2}\right)^2\right)^{1/2} \tag{83}$$

and the non-dimensional relationship with $\tau \to 0$ is

$$\Omega_{\mathrm{GWCE}} = \frac{1}{\pi}\sqrt{\frac{12\beta_2 + 4\beta_3}{\beta_1}} \tag{84}$$

and the non-dimensional surface is presented in Figure 9.

The dispersion surfaces in Figures 8 and 9 are typical of all the surfaces for the quasi-bubble and GWCE schemes. The monotonic behaviour described by the one-dimensional relationship carries over to the two-dimensional result, and in fact, a slice along the K_y-axis is identical to the one-dimensional result. However, a slice along the K_x-axis is not identical to the curve obtained from a one-dimensional derivation, but it is still monotonic. The reason for this is the 'staggering' of nodes in the x-direction and is fully explored in Atkinson

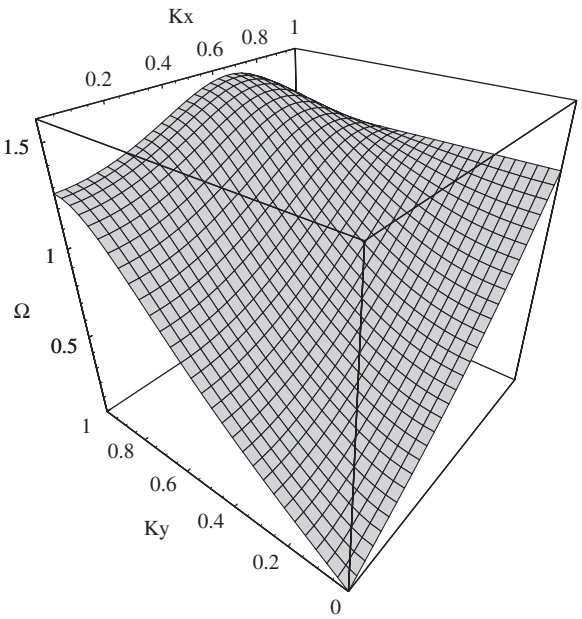

Figure 9. Two-dimensional dispersion surface for the GWCE scheme.

et al. [8]. It is significant that the GWCE and quasi-bubble schemes both possess monotonic dispersion properties for all directions, and it is this property that distinguishes them from many other schemes. For instance, a standard linear finite element discretization and many mixed interpolation approximations of the primitive shallow water equations possess folded dispersion relationships. As a consequence, these schemes cannot avoid oscillatory solutions. The well-documented success of the GWCE and quasi-bubble scheme is due to the monotone dispersion property.

4. NUMERICAL EXPERIMENTS

Numerical experiments are performed on the well-known quarter annular harbor test case [20] to verify the prediction that the two schemes will provide similar solutions when the value of G is appropriately chosen. Solutions were computed on the mesh shown in Figure 10, which corresponds to the patch of elements in Figure 6 that was used to construct the discrete equations. Simulations were performed for an M_2 wave with an amplitude of 5 ft (1.524 m) on the open boundary. The normal velocity is set to zero on the land boundary. Runs were made with bathymetry that varies quadratically from 10 ft (3.048 m) at the inner (land) boundary to 62.5 ft (19.05 m) at the outer (open) boundary. A small friction value of $\tau = 0.0001$ was defined. The GWCE computations were obtained with the Adcirc code [21], and the quasi-bubble calculations were obtained with the Telemac [14] computer code. A time step of 5 s was used for all calculations such that errors in the solution are dominated by the spatial discretization. For this small time step and within the range of depths in these simulations, the Courant number is very small and ranges from $Cr = 0.0018$ to 0.0045.

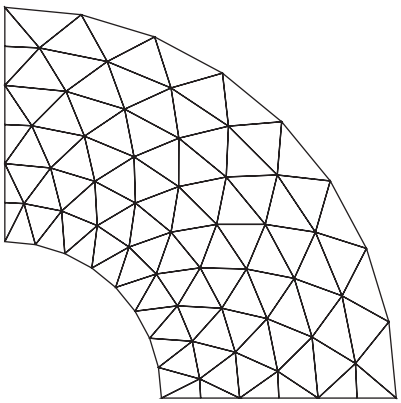

Figure 10. The computational mesh used for numerical experiments.

For this test case, the analytical solution is radially symmetric, so oscillations may be seen by plotting the maximum and minimum values at successive radial locations. The exact solution has four components, sine and cosine amplitudes for elevation and for radial velocity. Four plots are presented for each run. The solid line is the exact solution, and the symbols represent the maximum and minimum of the computed result at each radial location. Since the exact solution is radially symmetric, noisiness of the solution is revealed by the degree to which the maximum and minimum values deviate from each other.

Numerical results obtained with the quasi-bubble scheme are shown in Figure 11. There are no observable '$2\Delta x$' oscillations. The results are consistent with the two-dimensional dispersion analysis which predicts smooth solutions.

The first set of GWCE calculations was performed with $G = 0$. Results from calculations for $G = 0$ are shown in Figure 12 and are consistent with the dispersion analysis and demonstrate the monotonic dispersion properties of this scheme. None of the numerical solutions exhibit '$2\Delta x$' oscillations. Although the computed solution is radially symmetric and smooth, there is some deviation from the analytical solution for this value of G.

A second set of GWCE calculations was performed to test the findings of the previous section by comparing a GWCE computation with a value of G given by Equation (77) to the quasi-bubble results. The analysis was based upon the harmonic form of the governing equations which yields an imaginary G, but the computational codes are based upon the full equations. Thus, a real-valued coefficient must be used for the numerical experiments. The value

$$\begin{aligned} G &= \frac{(\hat{\mathrm{i}}\omega + 3\tau)}{2} \\ &= \left| \frac{\hat{\mathrm{i}}(0.0001405) + 3(0.0001)}{2} \right| \\ &\approx 0.0002 \end{aligned} \tag{85}$$

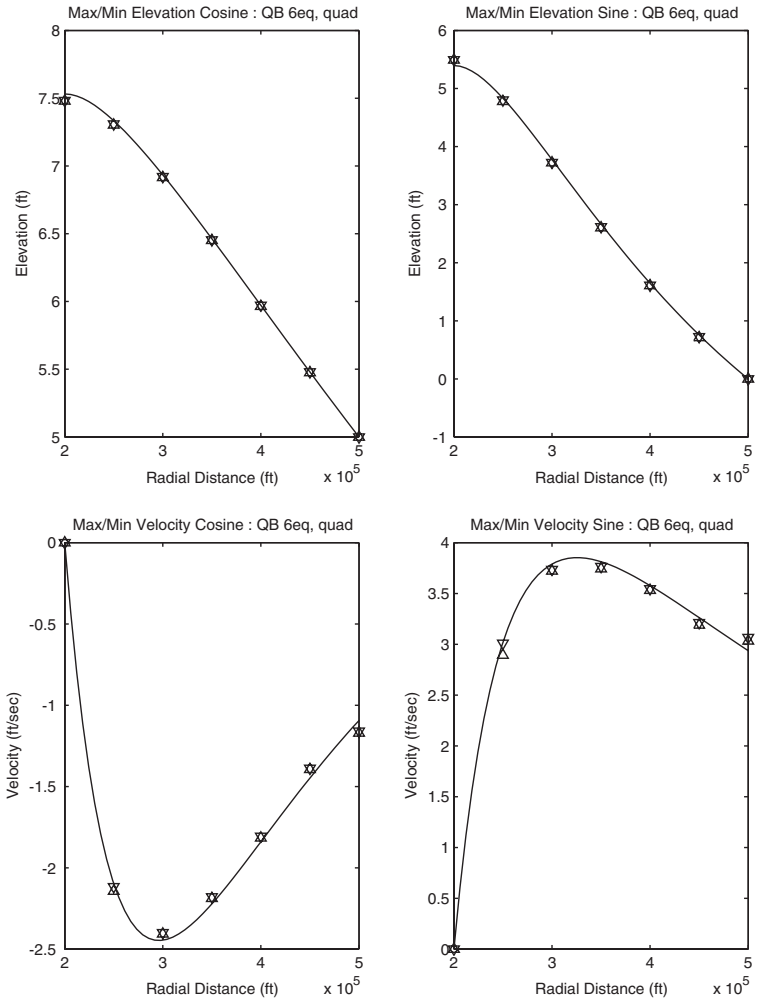

Figure 11. Results for the quasi-bubble scheme on the '6eq' grid with quadratic bathymetry.

was used for the Adcirc computations. The GWCE results are shown in Figure 13 and in fact are nearly identical to those obtained by the quasi-bubble-based Telemac model. This confirms the analysis by demonstrating the close similarity of the GWCE and quasi-bubble schemes when G is chosen appropriately. Also, note that the accuracy has improved greatly from the runs where $G = 0$, as shown in Figure 12. The improvement is due to the choice of G which brings the discrete dispersion relationship closer to the analytical relationship. This demonstrates that better results are obtained when the discrete dispersion surface is closer to the analytical dispersion surface. This case also demonstrates that the expression in Equation (77) defines an optimal G value and may be a useful tool for selecting the correct G balance.

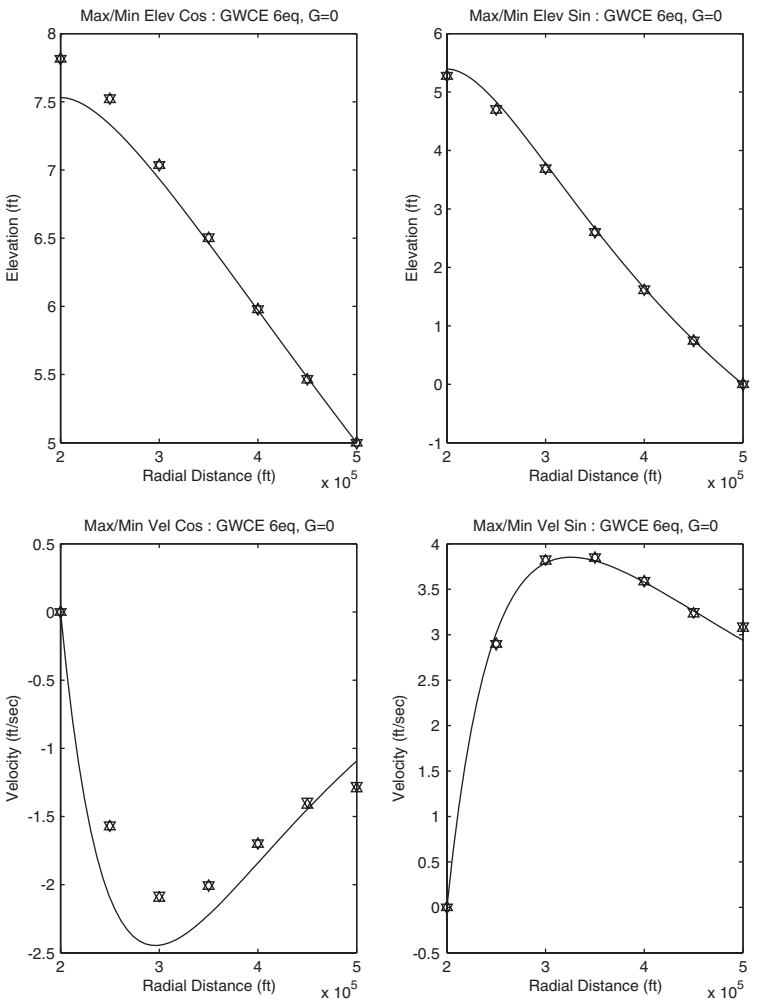

Figure 12. Results for the GWCE scheme on the '6eq' grid with quadratic bathymetry and $G = 0$.

5. CONCLUSIONS

Comparison of the discrete equations for the GWCE scheme and the quasi-bubble scheme has demonstrated that these schemes are very similar. Moreover, their discrete continuity stencils are shown to be identical for an appropriately selected value of G. The discrete momentum stencils are also very similar with the exception of the mass matrix. It is concluded that the quasi-bubble scheme is almost equivalent to the GWCE scheme with a specific weighting coefficient, G.

It is further demonstrated that the quasi-bubble scheme and the GWCE scheme with the G derived to make them equivalent, have dispersion properties that are near optimal. Empirical studies [19] for the optimal choice of G that balances smooth solutions and mass

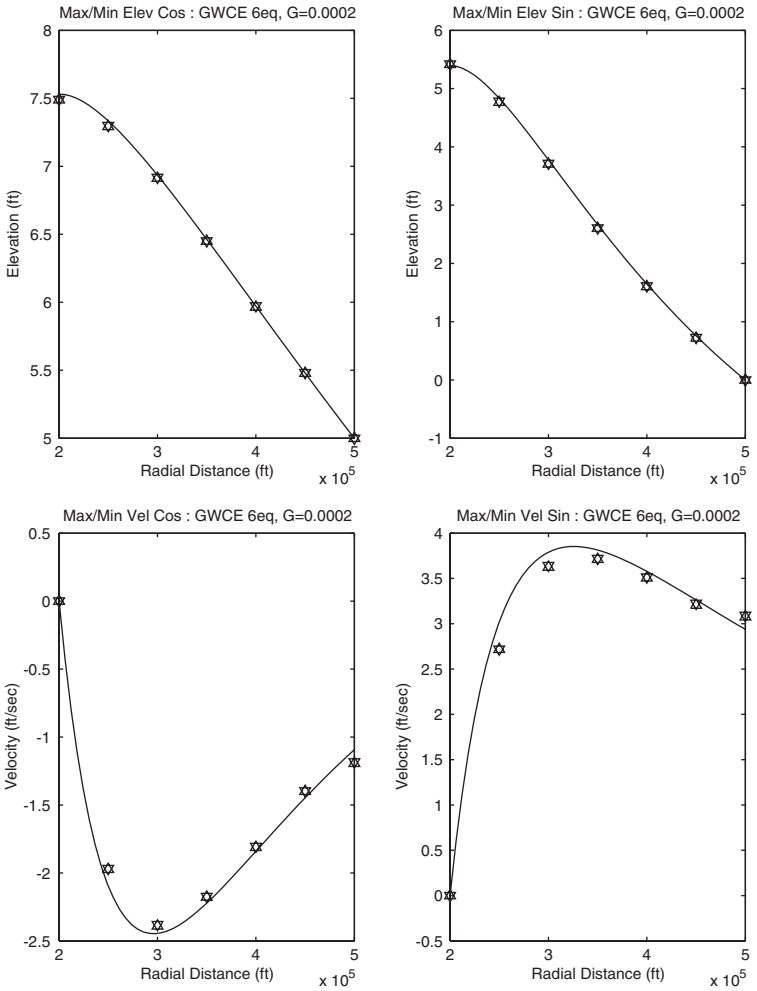

Figure 13. GWCE results with G = 0.0002 on the '6eq' grid and quadratic bathymetry.

conservation have suggested that G should be chosen proportional to the friction parameter τ and also has a lower limit. The relationships in Equations (41) and (77) imply the same balance and additionally suggest that the lower limit for G is proportional to the frequency. Two-dimensional dispersion surfaces for the GWCE scheme and the quasi-bubble scheme have also been presented. Both are entirely monotonic and very similar. Both schemes exhibit grid- and direction-independent propagation behaviour, which is an ideal property. Additionally, dispersion properties remain similar for one-dimensional and two-dimensional implementations. Numerical results for the quarter annular test problem are consistent with the dispersion analysis and demonstrate the excellent dispersion properties of these schemes. In fact it is clear that the G specified using Equation (77) leads to the best possible GWCE solution and is almost identical to the quasi-bubble solution.

The analyses presented here allows immediate improvement in GWCE-based codes through the identification of a G value with near optimal properties. In addition, this study explains that the success of the quasi-bubble algorithm is due to its excellent dispersion properties.

ACKNOWLEDGEMENTS

This research was supported by the U.S. Army Engineer Research and Development Center under contract DACW 42-00-C-0006 under the Coastal Inlets Research Program with Dr Nicholas Kraus as technical leader and Ms Mary Cialone as principal investigator.

REFERENCES

1. Kolar RL, Westerink JJ. A look back at 20 years of gwc-based shallow water models. In *Proceedings of the XIII International Conference on Computational Methods in Water Resources*, Calgary, Alberta, Canada, 2000; 899–906.
2. Westerink JJ, Gray WG. Progress in surface water modeling. *Reviews of Geophysics* (Suppl.). American Geophysical Union, April 1991; 210–217.
3. Kinnmark IP. *The Shallow Water Wave Equations*: *Formulation*, *Analysis and Application*. Springer; Berlin, 1986.
4. Hervouet JM. On spurious oscillations in primitive shallow water equations. In *Proceedings of the XIII International Conference on Computational Methods in Water Resources*, Calgary, Alberta, Canada, 2000; 929–936.
5. Lynch DR, Gray WG. A wave equation model for finite element tidal computations. *Computers and Fluids* 1979; **7**:207–228.
6. Kinnmark IP, Gray WG. A two-dimensional analysis of the wave equation model for finite element tidal computations. *International Journal for Numerical Methods in Engineering* 1984; **20**:369–383.
7. Kinnmark IP, Gray WG. Stability and accuracy of spatial approximations for wave equation tidal models. *Journal of Computational Physics* 1985; **60**:447–466.
8. Atkinson JH, Westerink JJ, Luettich RA. Two-dimensional dispersion analysis of finite element approximations to the shallow water equations. *International Journal for Numerical Methods in Fluids* 2004; **45**:715–749.
9. Platzman GW. Some response characteristics of finite element tidal models. *Journal of Computational Physics*, 1981; **40**:36–63.
10. Westerink JJ, Luettich RA, Wu JK, Kolar RL. The influence of normal flow boundary conditions on spurious modes in finite element solutions to the shallow water equations. *International Journal for Numerical Methods in Fluids* 1994; **18**:1021–1060.
11. Mewis P, Holtz KP. A quasi bubble-function approach for shallow water waves. In *Advances in Hydro-Science and Engineering*; *Proceedings of the First International Conference on Hydro-Science and Engineering*, Washington, D.C., U.S.A., vol. 1. 1993; 768–774.
12. Bates PD, Anderson MG, Hervouet JM, Hawkes JC. Investigating the behaviour of two-dimensional finite element models of compound channel flow. *Earth Surface Processes and Landforms* 1997; **22**:3–17.
13. Daubert O, Hervouet JM, Jami A. Description of some numerical tools for solving incompressible turbulent and free surface flows. *International Journal for Numerical Methods in Engineering* 1989; **27**:3–20.
14. Galland JC, Goutal N, Hervouet JM. Telemac: A new numerical model for solving the shallow water equations. *Advances in Water Resources* 1991; **14**:138–148.
15. Foreman MGG. An analysis of two-step time discretizations in the solution of the linearized shallow water equations. *Journal of Computational Physics* 1983; **51**:454–483.
16. Gray WG, Lynch DR. On the control of noise in finite element tidal computations. *Computers and Fluids* 1979; **7**:47–67.
17. Walters RA, Carey GF. Analysis of spurious oscillation modes for the shallow water and navier-stokes equations. *Computers and Fluids* 1983; **11**:51–68.
18. Leopoldo P. Franca, Charbel Farhat. On the limitation of bubble functions. *Computer Methods in Applied Mechanics and Engineering* 1994; **117**:225–230.
19. Kolar RL, Westerink JJ, Cantekin ME, Blain CA. Aspects of nonlinear simulations using shallow-water models based on the wave continuity equation. *Computers and Fluids* 1994; **23**:523–538.
20. Lynch DR, Gray WG. Analytical solutions for computer flow model testing. *Journal of the Hydraulics Division*, ASCE 1978; **104**:1409–1428.
21. Luettich RA, Westerink JJ, Scheffner NW. Adcirc, an advanced three-dimensional circulation model for shelves, coasts, and estuaries. *Technical Report*, U.S. Army Corps of Engineers, 1992.

